JOC The Journal of Organic Chemistry

Article

pubs.acs.org/joc

Insights into Stereoselective Aminomethylation Reaction of α,β-Unsaturated Aldehyde with N,O-Acetal via N-Heterocyclic Carbene and Brønsted Acid/Base Cooperative Organocatalysis

Yang Wang, Mingsheng Tang, Yanyan Wang, and Donghui Wei*

The College of Chemistry and Molecular Engineering, Center of Computational Chemistry, Zhengzhou University, Zhengzhou, Henan Province 450001, P.R. China

Supporting Information

ABSTRACT: A theoretical investigation has been performed to interrogate the mechanism and stereoselectivities of aminomethylation reaction of α,β-unsaturated aldehyde with N,O-acetal, which is initiated by N-heterocyclic carbene and Brønsted acid (BA). The calculated results disclose that the reaction contains several steps, i.e., formation of the actual catalysts NHC and Brønsted acid $Et_3N{\cdot}H^+$ coupled with activation of C−O bond of N,O-acetal, nucleophilic attack of NHC on α,β-unsaturated aldehyde, formation of Breslow intermediate, β-protonation for the formation of enolate intermediate, nucleophilic addition on the Re/Si face to enolate by the activated iminium cation, esterification coupled with regeneration of $Et_3N{\cdot}H^+$, and dissociation of NHC from product. Addition on the prochiral face of enolate should be the stereocontrolling step, in which the chiral α-carbon is formed. Furthermore, NBO, GRI, and FMO analyses have been performed to explore the roles of catalysts and origin of stereoselectivity. Surprisingly, the added Brønsted base (BB) Et_3N plays an indispensable role in the esterification process, indicating the reaction proceeds under NHC-BA/BB multicatalysis rather than NHC-BA dual catalysis proposed in the experiment. This theoretical work provides a case on the exploration of the special roles of the multicatalysts in NHC chemistry, which is valuable for rational design on new cooperative organocatalysis.

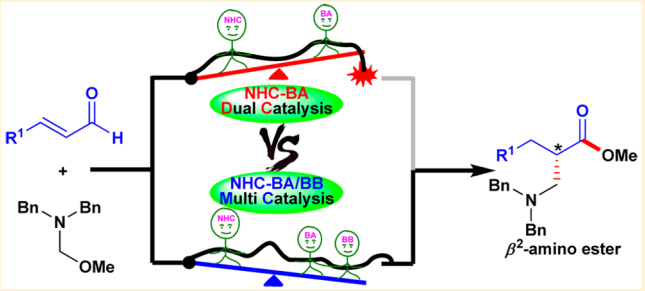

1. INTRODUCTION

In addition to biocatalysis and metal catalysis, organocatalysis has been recognized as the "third pillar" of asymmetric catalysis,[1] and is being increasingly used in the key steps in the total synthesis of complex natural products. In recent years, new and highly enantioselective processes were developed by using organocatalysis, which greatly expanded the scope of asymmetric organic synthesis.[2] Commonly, there were mainly four types of organocatalysts, including Lewis bases (LB), Lewis acids (LA), Brønsted acids (BA), and Brønsted bases (BB),[1] which were compatible with many different functional groups and provide high and predictable enantioselectivities for a wide rage of substrates. However, with the high-speed development in this field, various functions of organocatalysts have been identified by both experimental and theoretical studies, and the classifications of organocatalysts are far greater than the four types above used nowadays.[3] Thus, exploring the roles of catalyst and the general principle of the complicated organocatalysis would be the key for rational design of the new type of organocatalytic reaction with high selectivities in the near future.

Recently, cooperative organocatalysis appeared to be a promising new strategy for asymmetric synthesis, which relied on combining the advantages of both organocatalysis and multicatalysis in a one-pot reaction condition. In the case of cooperative organocatalysis, many options exist that result in high stereoselectivity by using the different functional organocatalysts coupled with the other acid/base as cocatalyst. As the well-known Lewis base organocatalyst, the N-heterocyclic carbene (NHC) has been widely employed in cooperative organocatalysis, which offers interesting opportunities for the discovery of new synthetic protocols. In 2010, Scheidt et al. made a significant breakthrough on the NHC in conjunction with Lewis acid $Mg(Ot\text{-}Bu)_2$ for an enantioselective addition of homoenolate intermediates to N-benzoyl hydrazones, in which the HOMO/LUMO energies of the substrates enals/N-benzoyl hydrazones are raised/lowered by NHC/LA, respectively (Scheme 1A).[4] Since then, various Lewis acids, such as $Ti(OiPr)_4$,[5] $Sc(OTf)_3$,[6] LiCl,[5a,7] and $La(OTf)_3$,[8] were also utilized to improve the reactivity of the different substrates in the NHC-LA cooperative organocatalysis. Subsequently, other kinds of cooperative organocatalytic systems including NHC-LB and NHC-BA were exploited for the annulation reactions of enals by Chi,[9] Rovis,[10] and other groups.[11] In 2013, Chi et al. pioneered a novel method on the enantioselective sulfonation reaction of enones with sulfonyl imines via cooperative NHC-thiourea/amine multicatalysis, in which the NHC played the

Received: March 28, 2016
Published: June 6, 2016

DOI: 10.1021/acs.joc.6b00656
J. Org. Chem. 2016, 81, 5370−5380

Scheme 1. Representative Reactions via the Cooperative Organocatalysis

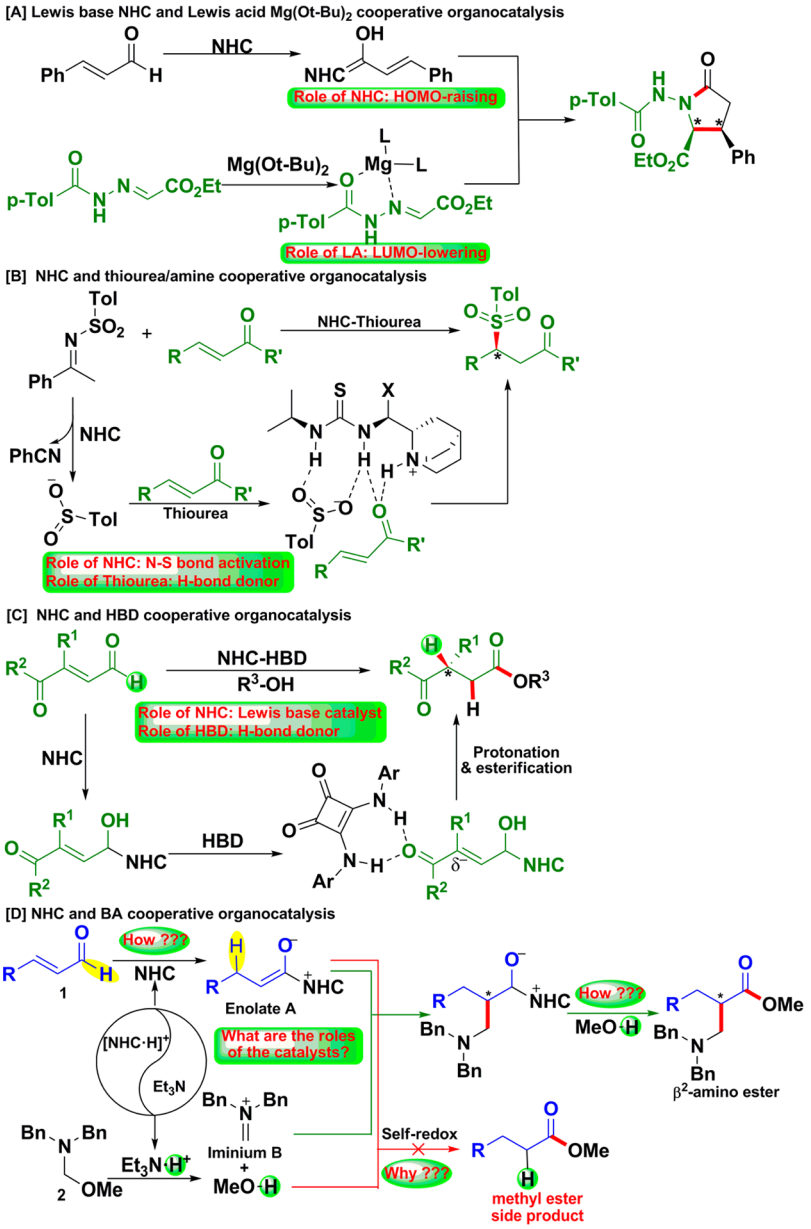

role of activation of the N−S bond rather than the Lewis base catalyst whereas the thiourea/amine worked as the hydrogen bond donor (Scheme 1B).[12] In addition, Scheidt and co-workers reported an enantioselective NHC-HBD (H-bond donor) cooperatively organocatalyzed β-protonation reaction of α,β-unsaturated aldehydes, in which the NHC served as Lewis base catalyst and the cocatalyst worked as the hydrogen bond donor (Scheme 1C).[13]

In 2015, Chi's group reported an outstanding example of the concise and highly stereoselective aminomethylation reaction of α,β-unsaturated aldehyde with N,O-acetal for the formation of β^2-amino acids and their derivatives, which was initiated under the NHC and Brønsted acid cooperative catalysis (Scheme 1D).[14] Before this report, the asymmetric synthesis of β^2-amino acids via catalytic approaches was limited, so it is highly desired to develop a facile and enantioselective route for the extensive preparation of β^2-amino acids and their derivatives. Thus, this kind of cooperative organocatalysis can be reasonably expected as one of the most important strategies for the synthesis of non-natural amino acids. As described above, the role of NHC in the cooperative organocatalysis reactions (Scheme 1A−C) would not always work as a Lewis base, and the real role of NHC remains unclear in this novel kind of aminomethylation reaction depicted in Scheme 1D. Moreover, NHC-BA cooperatively organocatalyzed [3 + 2][15]/[4 + 2][9,16] annulations, and C(sp^3)-H activation[17] has been studied in both experiment and theory, and almost all were confirmed via the NHC-BA dual catalysis, but it cannot be ensured whether the title reaction still shares the similar NHC-BA dual catalysis mechanisms before the systemic study in theory.

In the experiment (Scheme 1D), Chi and coauthors have conducted much effort to propose the mechanism for the complex reaction, and their explorations are quite instructive. However, some key issues are still obscure and need to be settled. (1) As shown in Scheme 1D, the reaction involves the activations of two substrates including the α,β-unsaturated

DOI: 10.1021/acs.joc.6b00656
J. Org. Chem. 2016, 81, 5370−5380

aldehyde **1** and N,O-acetal **2** by NHC catalyst and an in situ generated Brønsted acid $Et_3N{\cdot}H^+$, respectively. How can the reaction happen in detail? (2) The enolate intermediate **A** would be formed through the proton transfer processes (i.e., [1,2]-proton transfer and [1,4]-proton transfer). Obviously, the extremely high energy barrier would be involved in the direct [1,2]-proton transfer process, which is because of the large strain associated with the three-membered ring. Thus, how does the [1,2]-proton transfer process occur? Actually, Yu and co-workers have confirmed that the protic media can assist the [1,*n*]-H shift by both DFT calculations and the isotopic labeling experiment.[18] Thus, the $Et_3N{\cdot}H^+$ or other protic media assisted proton transfer processes should be considered in this work. (3) Previous studies show that NHC might play different roles in the organocatalytic reactions, such as Lewis base,[15,16b,19] C−H bond activation (α-CH, β-CH, and γ-CH),[6,17,20] and polarity inversion.[21] Thus, we want to know whether the NHC works as Lewis base organocatalyst in this reaction. (4) Base Et_3N rather than the corresponding Brønsted acid $Et_3N{\cdot}H^+$ was directly added in the reaction, but which one should be the actual catalyst to initiate the reaction? (5) The generated MeOH can directly react with enolate **A** to form the hydrocinnamic acid ester via self-redox reaction, which is observed as the side reaction in the experiment. Thus, what are the main reasons that lead to this kind of chemoselectivity? (6) The most important and difficult question, which can mainly be solved by the theoretical calculations, is to uncover the stereoselectivity-determining step. (7) In order to design the new organocatalytic reactions with high stereoselectivity, it is also necessary to explore the factors that govern the stereoselectivity of the reaction. The above questions and our research interests in NHC catalysis[15−17,19,22] prompt us to give a computational study not only for clarifying the aminomethylation reaction mechanism in detail, but also for exploring the factors that govern the chemo- and stereoselectivity. We believe that the computational results should be important for understanding the cooperative organocatalysis, and thus provides valuable insights on the rational design for this kind of reaction.

In the present study, we aim to shed light on the mechanism, the origin of the chemo- and stereoselectivity, as well as the roles of the catalysts involved in the asymmetric aminomethylation reaction between α,β-unsaturated aldehyde and N,O-acetal, which is catalyzed by NHC and in situ generated Brønsted acid $Et_3N{\cdot}H^+$ catalysts.[14] As shown in Scheme 2, the

Scheme 2. Model Reaction Employed in the Calculations

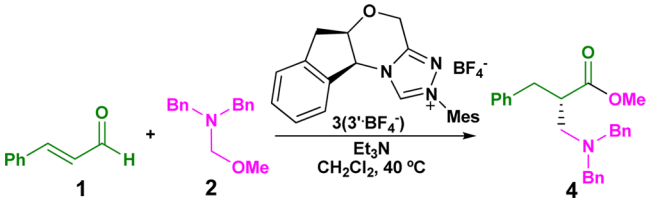

aminomethylation reaction between the α,β-unsaturated aldehyde **1** (**R1**) and N,O-acetal **2** (**R2**) catalyzed by the NHC **3′** (**Cat**) to afford the desired product β^2-amino esters **4** is chosen as the simulation model to investigate the detailed mechanism and stereoselectivity for this kind of reaction. Density functional theory (DFT), which has become the most prevalent and efficient tool for the theoretical studies to clarify favorable pathways, disclosing the origin of the stereoselectivity and/or chemoselectivity in the NHC catalyzed reactions,[15−17,19,22c,23] was employed to perform all the calculations in this work.

2. COMPUTATIONAL DETAILS

The Gaussian 09 suite of program[24] was employed for all the theoretical calculations. We selected the DFT method for this work, because of the successful applications on the mechanistic studies of the organic[22a,b,25] and biological reactions.[26] The complete geometry optimizations of all the stationary points were carried out at the M06-2X[27]/6-31G(d,p) level in DCM solvent using the SMD continuum solvation model[28] at 298 K and 1 atm. The same-level vibrational frequencies were then calculated to identify that there is no imaginary frequency in the local minima and only one imaginary frequency in each transition state. Subsequently, we performed intrinsic reaction coordinate (IRC)[29] calculations to ensure that the expected reactant and product are connected with the corresponding transition state. The natural population analysis (NPA)[30] and the CYLView software[31] were employed for computing the atom charges and rendering the 3-D structures, respectively. The energies discussed in this work are based on the Gibbs free energies obtained at the M06-2X/6-31G(d,p)//SMD_{DCM} level.

In addition, the single-point energies for the stereoselectivity-determining transition states were refined by using different methods and solvent models (i.e., ωB97X-D,[32] B3LYP,[33] and B3LYP-D3[34]), and the structures of the stereoselectivity-determining step were also reoptimized at the ωB97X-D/6-31G(d,p)//SMD_{DCM} and M06-2X/6-31G(d,p)//IEF-PCM_{DCM} levels to test the accuracy of the M06-2X/6-31G(d,p)//SMD_{DCM} level, the computational results were summarized in Tables S1−S3 of the Supporting Information. Compared with the results calculated at the M06-2X/6-31G(d,p)/SMD_{DCM} level, the computational outcomes obtained at the different levels mentioned above have the same trends and tiny differences; thus, we think the conclusions based on the results calculated at the M06-2X/6-31G(d,p)/SMD_{DCM} level are reliable.

3. RESULTS AND DISCUSSION

3.1. Reaction Mechanisms. Disclosed by Chi and co-workers, the experimental approach involved in the treatment of two reactants α,β-unsaturated aldehyde and N,O-acetal, and base Et_3N and the triazolium salt as the precatalysts.[14] Because all the reagents were mixed together in a one-pot reaction condition, the number of likely combinations between them can be envisaged to be proportionally higher as opposed to that in a sequential addition followed by synthetic manipulations of the intermediate compounds. Relying on the various sequences of combination of the substrates with catalysts, several possible mechanistic pathways for the fundamental reaction steps were considered in this work.

3.1.1. Formation of the Actual Catalysts and Substrates. As depicted in Scheme 3, the catalytic reaction initiates with the generation of two actual catalysts (i.e., NHC and $Et_3N{\cdot}H^+$), which is followed by the activation of C−O bond of N,O-acetal for the formation of iminium cation **B** and methanol by the deprotonation of the original precatalyst assisted by the added base Et_3N. The formation of the active catalysts **Cat** and $Et_3N{\cdot}H^+$ first occurs via abstracting the proton of the original **Pre-Cat** by Et_3N. This process is endergonic by 8.6 kcal/mol, which can occur under the experimental condition (40 °C). Subsequently, Brønsted acid $Et_3N{\cdot}H^+$ promotes the cleavage of O4−C5 bond in **R2** for the formation of two active species iminium cation **B** and methanol via transition state **TS0**. The free energy barrier of this step is 18.7 kcal/mol, indicating that the activation process can occur easily under the experimental condition.

DOI: 10.1021/acs.joc.6b00656
J. Org. Chem. 2016, 81, 5370−5380

Scheme 3. Generation of Two Actual Catalysts (NHC and $Et_3N{\cdot}H^+$) Accompanied with C−O Bond Activation Process[a]

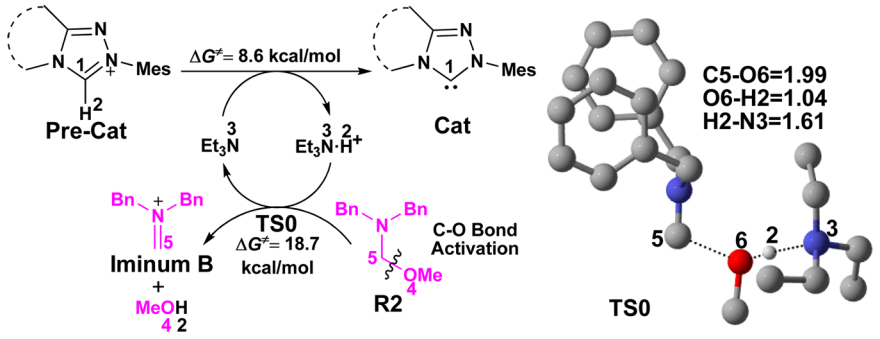

[a]Most of hydrogens are omitted for the sake of clarity. (Distance in Å and the energy profile are provided in Figure S1 of Supporting Information).

Scheme 4. Entire Cycle of Cooperative Organocatalysis

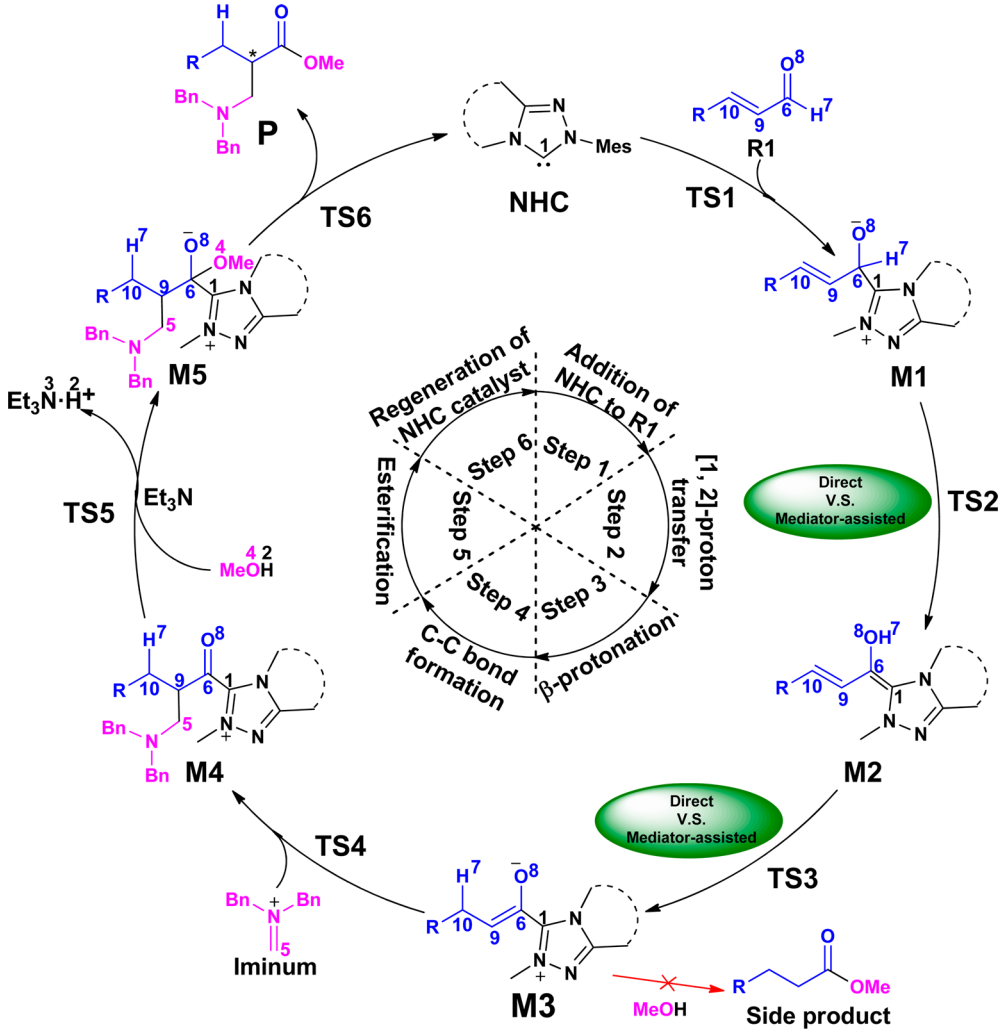

3.1.2. Catalytic Cycle. Starting from the formerly generated catalysts NHC and $Et_3N{\cdot}H^+$, we have suggested the possible catalytic cycle which includes the following six steps (Scheme 4). Initially, the nucleophilic addition of NHC on the electrophilic carbonyl carbon of **R1** gives a zwitterionic intermediate **M1** via transition state **TS1**. Subsequently, **M1** then transforms to the Breslow intermediate **M2** via the three-membered proton transfer transition state **TS2**, which is identified to be the well-recognized process involved in NHC catalyzed reactions. The following process is β-protonation of **M2** to afford the enolate intermediate **M3** through [1,4]-proton transfer. Then, it is the intermolecular Mannich reaction (C−C bond formation) between **M3** and iminium cation **B** for the generation of intermediate **M4**. Last, it is the esterification reaction mediated by Et_3N via transition state **TS5** for the formation of intermediate **M5**, which then directly dissociates to the desired β^2-amino ester product **P** and the NHC catalyst via transition state **TS6**. The corresponding free energy profile of the entire cycle involved in the most energy favorable reaction pathway has been illustrated by Figure 1, in which the

DOI: 10.1021/acs.joc.6b00656
J. Org. Chem. 2016, 81, 5370−5380

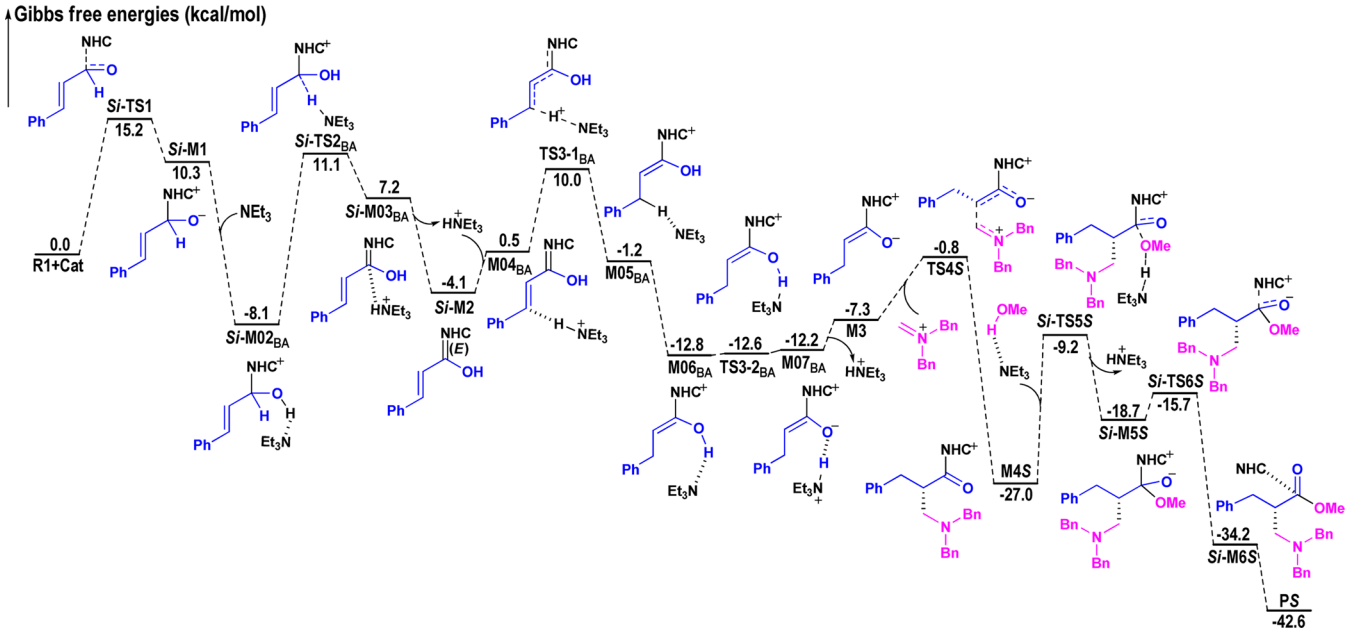

Figure 1. Gibbs free energy profile of the entire catalytic cycle (only the most energy favorable pathway was shown here, and the whole energy profile involved in all the possible reaction pathways was provided in the Supporting Information).

free energy of **R1**+**NHC** was set as 0.00 kcal/mol as reference. In the following parts, we will give a detailed discussion on the mechanistic perspective of this novel cooperative organocatalytic reaction.

*First Step. Addition of **NHC** to **R1**.* Due to the existence of prochiral face in the substrate **R1**, the zwitterionic intermediates ***Re***/***Si*-M1** generate via transition states ***Re***/***Si*-TS1** by the *Re*/*Si* face addition of **NHC** to **R1**, respectively (for details of *Re* face addition see the Supporting Information). In Figures 1 and S2, the Gibbs free energy barriers via ***Re***/***Si*-TS1** are 16.5/15.2 kcal/mol and the free energy barriers of intermediates ***Re***/***Si*-M1** are 10.3/10.3 kcal/mol, respectively.

Second Step. Formation of Breslow Intermediate. As is well-known in the related α,β-unsaturated aldehyde (or enal) reaction catalyzed by **NHC**, the formation of the Breslow intermediate is an important and common process. In this step, the proton H7 atom transfers from C6 atom to O8 atom to give intermediate **M2**. Many studies have verified that this is difficult to occur through the direct [1,2]-proton transfer because of the high energy barrier.[15,16,35] Our calculated results show the energy barriers of the process via ***Re***/***Si*-TS2$_D$** are 50.5 and 47.4 kcal/mol, respectively(more details can be found in Figure S3 of Supporting Information), revealing such a possibility is not likely to happen under the experimental condition.

It has been widely recognized that the proton transfer process could occur by a very low energy barrier when a protic media is invoked. Considering this point, we have then taken the $Et_3N{\cdot}H^+$ and methanol mediated proton transfer pathways into account. As shown in Scheme S1, there are three possible mediator-assisted proton transfer processes, including the Et_3N-assisted proton transfer process, $Et_3N{\cdot}H^+$-assisted proton transfer process, and methanol-assisted proton transfer process.

Based on our results, one can easily conclude that $Et_3N{\cdot}H^+$-assisted proton transfer process to form ***Si*-M2** via ***Si*-TS2$_{BA}$** (19.2 kcal/mol, Figure 1) is the most energetically feasible of the MeOH-assisted proton transfer mechanisms, mainly because of the stronger acidity of $Et_3N{\cdot}H^+$ ($pK_a \approx 10.3$) than MeOH ($pK_a \approx 16$). It should be noted that we only have the theoretical data in this study and do not have experimental evidence to support the discoveries in this paper. Furthermore, the relative energy of ***Si*-M2** ($\Delta G = -4.1$ kcal/mol, Figure 1) locates 4.8 kcal/mol lower than that of ***Re*-M2** ($\Delta G = 0.7$ kcal/mol, Figure 1), so we think it is not necessary to consider the possibility of the *Re* face attack on **R1**in the following parts.

Third Step. Formation of Enolate Intermediate. The next step is β-protonation of the Breslow intermediate **M2** to afford enolate intermediate **M3** through the proton H7 transfer from O8 to C10 atom. Three possible pathways, i.e., direct proton transfer pathway, $Et_3N{\cdot}H^+$-assisted proton transfer pathway, and MeOH-assisted proton transfer pathway (Scheme S2 of the Supporting Information), were studied in this step. We first investigated the direct proton transfer pathway (Scheme S2A of the Supporting Information), namely, the intermediate **M3** can be afforded via a [1,4]-proton transfer process associated with the five-membered ring transition state **TS3$_D$**. The direct proton transfer process costs 25.6 kcal/mol in free energy with respect to ***Si*-M2** (Figure S2 of the Supporting Information), which seems to be a little high. Consequently, we then considered the Brønsted acid $Et_3N{\cdot}H^+$- and MeOH-assisted proton transfer pathways (Schemes S2B and S2C of the Supporting Information). In the $Et_3N{\cdot}H^+$-assisted proton transfer pathway, intermediate **M04$_{BA}$** first forms and then H2 transfers to C10 atom via transition state **TS3−1$_{BA}$** to give intermediate **M05$_{BA}$**. The energy barrier of this pathway is 14.1 kcal/mol (Figure 1), which is remarkably lower than that of the direct proton transfer pathway. Subsequently, the intermediate **M06$_{BA}$** ($\Delta G = -12.8$ kcal/mol, Figure 1) forms, and the existence of the O−H···N hydrogen bond makes it more stable than **M05$_{BA}$** ($\Delta G = -1.2$ kcal/mol, Figure 1). The computational results indicate that H7 can easily transfer to the N3 atom via transition state **TS3−2$_{BA}$** to generate intermediate **M07$_{BA}$**, and finally enolate intermediate **M3** forms by removing the $Et_3N{\cdot}H^+$. The energy barrier of this step is only 0.2 kcal/mol (Figure 1), indicating that H7 abstraction can occur easily. It should be noted that the intermediate **M07$_{BA}$** is located 0.4 kcal/mol (Figure 1) higher than **TS3−2$_{BA}$**, while this difference

DOI: 10.1021/acs.joc.6b00656
J. Org. Chem. 2016, 81, 5370−5380

is reversed based on the total energy ($\Delta E_{M07BA-TS4BA}$ = −1.3 kcal/mol; for details see Supporting Information). For the MeOH-assisted proton transfer pathway, the enolate intermediate **M3** forms via a seven-membered ring transition state **TS3$_M$**. The free energy barrier of this pathway is 18.7 kcal/mol (Figure S2 of the Supporting Information), which is also more favorable than the direct pathway but less favorable than the $Et_3N{\cdot}H^+$-assisted proton transfer pathway. As above, the $Et_3N{\cdot}H^+$-assisted proton transfer pathway via transition states **TS3−1$_{BA}$** ($\Delta G^{\neq}$ = 14.1 kcal/mol, Figure 1) and **TS3−2$_{BA}$** ($\Delta G^{\neq}$ = 0.2 kcal/mol, Figure 1) is found to be the most energy favorable.

Fourth Step. C−C Bond Formation. In this step, the previously generated enolate intermediate **M3** behaves as a nucleophilic substrate to undergo a Mannich reaction with iminium cation **B**. By electrostatic attraction between C9 and C5, a C−C single bond is formed in intermediates **M4*R*/*S*** via transition states **TS4*R*/*S*** (Scheme 4). Due to the existence of the prochiral face of **M3**, the C−C single bond can be constructed by *Re*/*Si* face addition of **M3** by the reactive iminium cation **B**, and concurrently, the chirality of carbon C9 emerges during the C−C bond formation. The *Re* face addition of **M3** leads to the *S*-configurational intermediate **M4*S***, while the *Si* face addition of **M3** contributes to the *R*-configurational intermediate **M4*R***. As depicted in Figure 1, the free energy barriers of **TS4*R*** and **TS4*S*** are 10.5 and 6.5 kcal/mol, respectively. Compared with the enantioselective pathways, the pathway associated with **TS4*S*** (6.5 kcal/mol) is more energy favorable than that via **TS4*R*** (10.5 kcal/mol), indicating that the formation of *S* configuration intermediate **M4*S*** is prior to the formation of *R* configuration intermediate **M4*R*** in this step. Moreover, the free energies of **M4*R*/*S*** are −22.8/−27.0 kcal/mol, and the intermediate **M4*S*** is obviously more energetically stable than **M4*R***. Combining those discussions, the attacking on the *Re* face of **M3** is the main pathway and the *S* configuration of the C9 chiral center is dominant. These findings align well with the experimental observations.

Fifth Step. Nucleophilic Addition of Methanol. As shown in Scheme 4, since the intermediates **M4*R*/*S*** have been formed in the fourth step, the following step is the nucleophilic addition of methanol to construct the desired β^2-amino ester product via transition state **TS5** (Figure 2). The free energy profiles depicted in Figures 1 and **S1** show that the free energy barriers of this step are 31.28 kcal/mol (***Re*-TS5*R***, Figure S2), 18.1 kcal/mol (***Si*-TS5*R***, Figure S2), 20.2 kcal/mol (***Re*-TS5*S***, Figure S2), and 17.8 kcal/mol (***Si*-TS5*S***, Figure 1), respectively, which implies that the *Si* face addition by methanol is more feasible than the *Re* face addition, and this also supports the preference to form the *S* isomer of the product.

*Sixth Step. Regeneration of the **NHC**.* As depicted in Figure 1, the free energy barrier of the last dissociation of NHC and product **P** is 3.0 kcal/mol via transition state ***Si*-TS6*S***, revealing that the regeneration of catalyst is a facilitated process.

3.1.3. Self-Redox Reaction. As shown in Scheme 1, the side reaction (i.e., self-redox conversion reaction) between the enolate intermediate **M3** and methanol would occur for the formation of hydrocinnamic acid methyl ester. Figure 3 shows the whole process of the self-redox reaction. Since aminomethylation reaction and self-redox reaction share the same formation process of enolate intermediate, and diverge afterward, we investigated the steps of self-redox reaction following from the enolate intermediate **M3**. The O4 atom of methanol first attacks the C6 atom in **M3**, accompanied by the

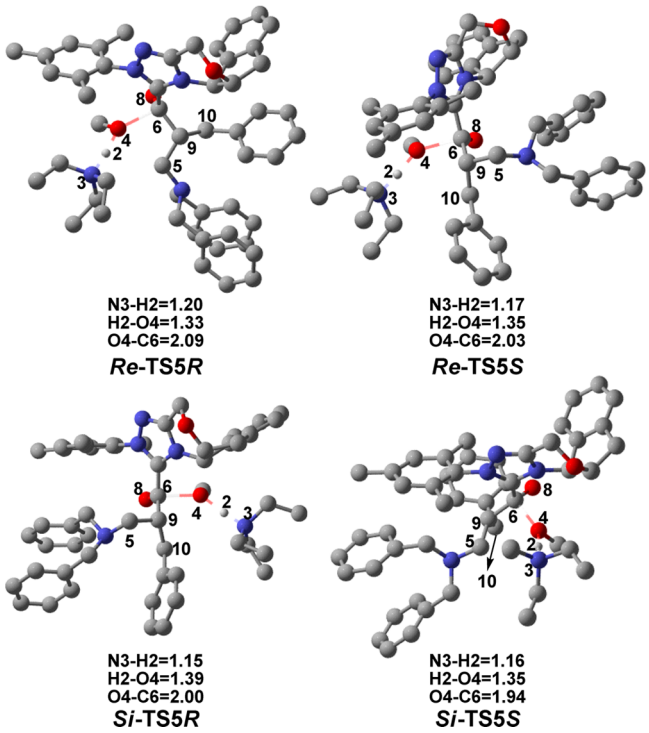

Figure 2. Optimized 3-D structures involved in the fifth step (distance in Å and most of the hydrogens are omitted for the sake of clarity).

protonation of the C9 atom to give the methyl ester intermediate **M4$_S$**.

Similar to the reaction between **M3** and iminium cation **B**, there are also two possible reaction patterns for this step, because the MeOH can also attack the Re/Si face of M3 for the formation of ***Re*/*Si*-M4$_S$**. Next, the obtained intermediates ***Re*/*Si*-M4$_S$** undergo rapid dissociation via transition states ***Re*/*Si*-TS5$_S$** to afford the hydrocinnamic acid methyl ester product **P$_S$**, which is also accompanied by the regeneration of the catalyst **NHC**. The MeOH addition step has the highest energy barrier (25.6/26.4 kcal/mol) based on the overall free energy profile for the self-redox reaction (Figure 3). In addition, we have also considered the Brønsted acid $Et_3N{\cdot}H^+$-assisted side esterification mechanism, in which the Brønsted acid $Et_3N{\cdot}H^+$ first protonates the α-carbon of enolate intermediate **M3** (Figure S8 of Supporting Information). However, the calculated outcomes reveal that the energy barrier of the protonation process is 33.2 kcal/mol, indicating that the $Et_3N{\cdot}H^+$-assisted side reaction is impossible under the experimental conditions. This results show that both addition modes are more unfavorable than those pathways of the reaction between **M3** and iminium cation **B**, revealing that the side reaction is kinetically unfavorable.

Furthermore, we have additionally investigated the other side reaction (i.e., the enal dimerization; for details see Figure S9 of Supporting Information) based on Bode's work,[21a] in which the Breslow intermediate ***Si*-M2** reacts with another molecule of α,β-unsaturated aldehyde (enal). Herein, we have only considered the reaction pathway associated with the main product (*RR* configuration) reported in Bode's work. The computational results show that the energy barrier of the enal dimerization reactions associated with transition state **TS3*RR*$_S$** is 17.9 kcal/mol (see Figure S9 of the Supporting Information), which is obviously higher than that of the β-protonation process to form **M3** (14.1 kcal/mol, Figure 1). Thus, we think

DOI: 10.1021/acs.joc.6b00656
J. Org. Chem. 2016, 81, 5370−5380

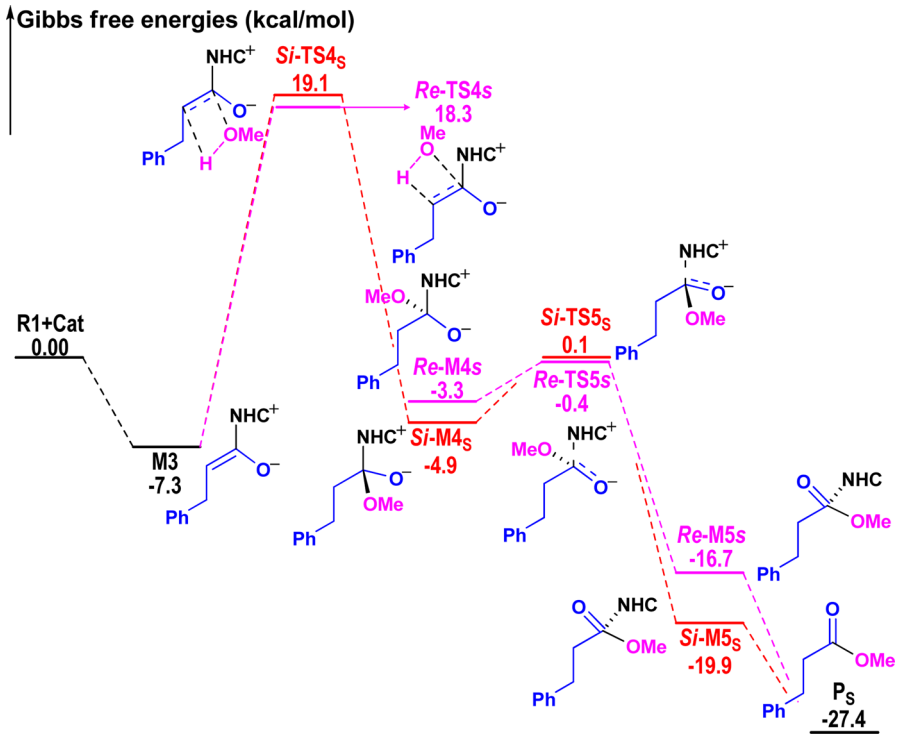

Figure 3. Gibbs free energy profile of the self-redox reaction.

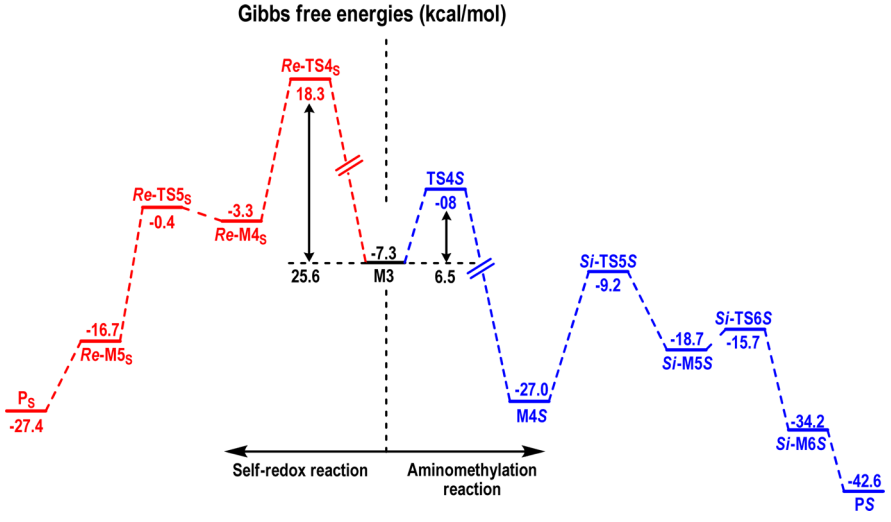

Figure 4. Comparison between aminomethylation reaction and self-redox reaction.

the enal dimerization reaction is kinetically unfavorable to the proton transfer process.

3.2. Origin of Chemoselectivity and Enantioselectivity. Disclosing the origin of stereoselectivity and chemoselectivity based on the established mechanism is important for an organocatalytic reaction. As discussed above, the proton transfer processes (i.e., the second and third steps of the catalytic cycle) contain more than one pathway. In both the second and third steps, the $Et_3N{\cdot}H^+$-assisted proton transfer processes associated with transition states ***Si*-TS2$_{BA}$** and ***Si*-TS3-1$_{BA}$** are the most favorable. In the last three steps, the *Si* face addition of **M3** by iminium cation **B** leading to product **PS** is the main reaction pathway. Moreover, the chirality center (C9 atom) emerges in the Mannich reaction step (the fourth step) and the side reaction could also occur in this step, so this step should be both the enantioselectivity- and chemoselectivity-determining step (β^2-amino ester product generates preferentially and *S*-configuration is predominant).

Discussions on the Chemoselectivity. Due to the special activity of the enolate intermediate, it can precede two competing reactions: one is aminomethylation reaction leading to the desired final product β^2-amino ester, and the other one is the self-redox reaction leading to the side product hydrocinnamic acid methyl ester. The aminomethylation reaction and self-redox reaction diverge from the enolate intermediate **M3** (Figure 4). Herein, we use the energetic span model[36] to compare the aminomethylation reaction with the self-redox reaction. The enolate intermediate **M3** is the turnover frequency determining intermediate (TDI) for the aminomethylation reaction and self-redox reaction. For the amino-

DOI: 10.1021/acs.joc.6b00656
J. Org. Chem. 2016, 81, 5370−5380

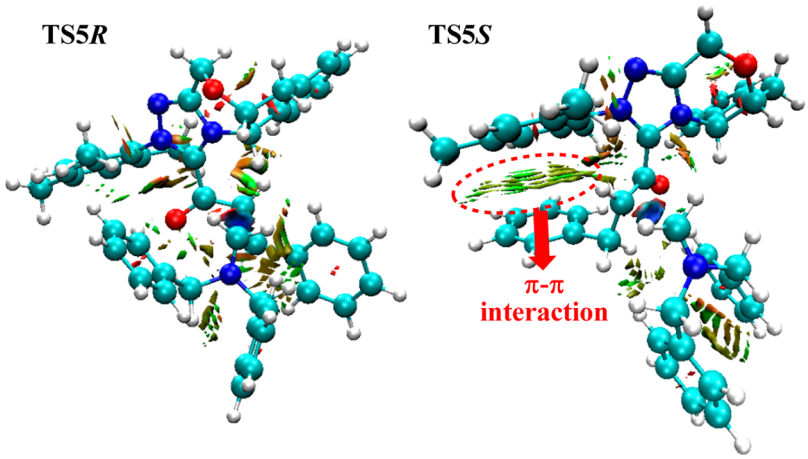

Figure 5. Interaction analysis of the transition states **TS5*R*** and **TS5*S*** (green, blue, and red represent weak, strong, and repulsive interactions, respectively.).

Table 1. Energies of HOMO (E_H, a.u.) and LUMO (E_L, a.u.), Electronic Potential (μ, a.u.), Chemical Hardness (η, eV), Global Electrophilicity (ω, eV), and Global Nucleophilicity (N, eV) of R1, *Re*/*Si*-M1, and M3

SR	E_H	E_L	μ	η	ω	N
R1	−0.28072	−0.03783	−0.159275	0.24289	1.42	2.47
***Re*-M1**	−0.24356	0.00311	−0.120225	0.24667	0.80	3.49
***Si*-M1**	−0.24510	0.00709	−0.119005	0.25219	0.76	3.44
M3	−0.21535	0.00153	−0.10691	0.21688	0.72	4.25

methylation reaction, the transition state **TS4*S*** with the related δE (6.4 kcal/mol, Figure 4) is the turnover frequency-determining transition state (TDTS), considering that the C−C bond formation process is irreversible. For the self-redox reaction, the transition state ***Re*-TS4$_S$** is the TDTS, and the related δE is 25.6 kcal/mol (Figure 4). Therefore, the δE of the aminomethylation reaction is much smaller than that for the self-redox reaction, and the aminomethylation reaction has a larger TOF. In addition, the product of the aminomethylation reaction (**PS** associated with the energy of −42.6 kcal/mol) is more thermodynamically stable than the product of self-redox reaction (**PS** associated with the energy of −27.4 kcal/mol). Moreover, comparing the free energy barriers of the aminomethylation reaction with those of self-redox reaction, one can conclude that the Gibbs free energies associated with the nucleophilic attack of the enolate intermediate by activated iminium cation are 6.5 kcal/mol (**TS5*S***) and 10.5 kcal/mol (**TS5*R***), respectively, while the Gibbs free energies of the self-redox reaction are 25.6 kcal/mol (***Re*-TS4$_S$**) and 26.4 kcal/mol (***Si*-TS4$_S$**), respectively. Obviously, the nucleophilic attack of the enolate intermediate by an activated iminium cation is more energetically preferred than the self-redox reaction. Thus, we think the aminomethylation reaction is kinetically and thermodynamically more favored than the self-redox reaction, and this conclusion is in agreement with experimental observations, where the β^2-amino ester product was obtained predominantly. Furthermore, the highly exergonic nucleophilic attack (i.e., the thermodynamic stability of **M4S**) and the facile subsequent steps in the aminomethylation reaction result in the feasibility of the formation of a β^2-amino ester product.

Discussions on the Enantioselectivity. In addition, we decided to pursue a deeper understanding of the enantioselectivity induced by the chiral catalyst NHC and Brønsted acid $Et_3N{\cdot}H^+$ through DFT calculations. As discussed above, the nucleophilic attack of the enolate intermediate **M3** on the iminium cation **B** determines the stereoselectivity of the aminomethylation reaction. The attacking *Re* face of **M3** by iminium cation **B** leads to the *S*-configurational product, while the attacking *Si* face of **M3** contributes to the *R*-configurational product and the corresponding transition states are **TS5*R*** and **TS5*S***, respectively. The Gibbs free energies of the two transition states are 11.8 and 6.4 kcal/mol, respectively. Therefore, the *Re* attack mode leading to the *S*-configurational product (**PS**) is more favorable.

To explore the origins of the enantioselectivity of the aminomethylation, we further carried out the noncovalent interaction (NCI) analysis,[37] which is extensively applied for recognizing intermolecular interactions. As shown in Figure 5, the $\pi-\pi$ interaction between benzyl group and mesityl group is identified to be the main factor for determining the preferential formation of the *S*-configuration product. The relative Gibbs free energy of **TS5*R*** is calculated to be 4.0 kcal/mol higher than **TS5*S***, which is consistent with the experimental results.

3.3. Roles of the Catalysts (NHC and $Et_3N{\cdot}H^+/Et_3N$).

Having located the most energy favorable reaction pathway, we now turn to exploring the special roles of the NHC catalyst and additives in this novel aminomethylation reaction, which should be valuable for rational design of other cooperatively organocatalytic reactions.

*Role of the **NHC**.* The NBO analysis has first been carried out before and after the absorption of NHC catalyst. The NBO charge assigned on the H7 slightly changes from 0.173 *e* in **R1** to 0.192 *e* in ***Si*-M1**, indicating that the acidity of the carbonyl C−H has been enhanced by NHC, which facilitates the C−H activation. Thus, one of the important roles for NHC is to activate the C−H bond by strengthening its acidity in this kind of reaction.

Based on global reactivity index (GRI) analysis, the NHCs have been confirmed to work as Lewis base organocatalysts in the cycloaddition and some annulation reactions.[15,16b,19]

DOI: 10.1021/acs.joc.6b00656
J. Org. Chem. 2016, 81, 5370−5380

Herein, we also employed the GRI analysis to disclose whether the NHC works as Lewis base in this reaction. In GRI analysis, the molecule's global electrophilicity character (ω)[38] and an empirical nucleophilicity index N[39] introduced by Domingo et al. were employed to explain the reactivities of the reactants. As summarized in Table 1, we can conclude that the electrophilicity of **R1** is slightly decreased by coordination of NHC, whereas the nucleophilicity of **R1** (2.47 eV) is increased remarkably, and the values of nucleophilicity are 3.49, 3.44, and 4.25 eV associated with ***Re*/*Si*-M1** and enolate intermediate **M3**, respectively. Thus, the GRI analysis also confirms that another role of NHC catalyst is Lewis base in the reaction.

As discussed above, the NBO and GRI analyses demonstrate that NHC catalyst plays dual roles in the reaction system. During the β-protonation process, the role of the NHC catalyst is to activate the inert carbonyl C−H bond. While in the aminomethylation process, the NHC mainly works as a Lewis base catalyst to strengthen the nucleophilicity of the substrate, especially the nucleophilicity of the enolate intermediate **M3**. Inspired by Yu's study,[40] we have also explored the relationship between nucleophilicity and HOMO energy of nucleophile **M3**. As shown in Figure S10 of the Supporting Information, there is a linear relationship between the nucleophilicity (N_j) and HOMO energy (H_j) of the nucleophile with the different substituents, which is in good agreement with Yu's study. In addition, it is obvious that the energy barriers would decrease when the nucleophilicities of the nucleophiles with different substituents in the same position increase (see Figure S11 of Supporting Information).

Role of the Brønsted Acid/Base ($Et_3N{\cdot}H^+$/Et_3N). The in situ generated $Et_3N{\cdot}H^+$ and its conjugated base Et_3N are mainly involved in three processes of the reaction, namely, the C−O bond activation process, proton transfer process, and esterification process. So the Brønsted acid/base should play a different role in each process.

Hydrogen Bond Donor ($Et_3N{\cdot}H^+$) to Facilitate Activation of the C−O Bond. In the C−O bond activation process, the bond length of C5−O4 is slightly lengthened from 1.41 Å in **R2** to 1.44 Å in the reaction precursor **Pre-M0**, and the bond orders of the C5−O4 bond are 0.74 and 0.69 in **R2** and **Pre-M0**, respectively. Actually, we have failed to locate the direct dissociation transition state of N,O-acetal, and we have scanned the length of the C5−O4 bond. The scanning result (Figure S12 in Supporting Information) shows that the dissociation energy of C5−O4 bond keeps increasing when the iminium cation **B** is moving away from the MeO^-. The dissociation energy is estimated to be not lower than 59.6 kcal/mol, which should be much higher than that of N,O-acetal. These findings reveal that the $Et_3N{\cdot}H^+$ is important and necessary in the C−O bond activation process, in which it works as a hydrogen bond donor to weaken the C−O bond, facilitating the subsequent cleavage of the C−O bond.

Proton Transfer Mediator to Promote the Formation of Breslow and Enolate Intermediates. As for the proton transfer processes, their energy barriers are lowered significantly by using $Et_3N{\cdot}H^+$ as protic mediator (Figure 1). Thus, the $Et_3N{\cdot}H^+$ mainly works as proton transfer mediator to facilitate these two proton transfer processes, which should be the reason that the $Et_3N{\cdot}H^+$ is acidic enough to protonate the Breslow intermediate at the β-position.

Hydrogen Acceptor (Et_3N) to Promote the Esterification Process. In the esterification process, the Brønsted base (Et_3N) participates in the reaction eventually transforming to the Brønsted acid $Et_3N{\cdot}H^+$. As shown in Figure 6, the 2p orbital of the O4 atom would overlap with the 2p-orbital of the C6 atom

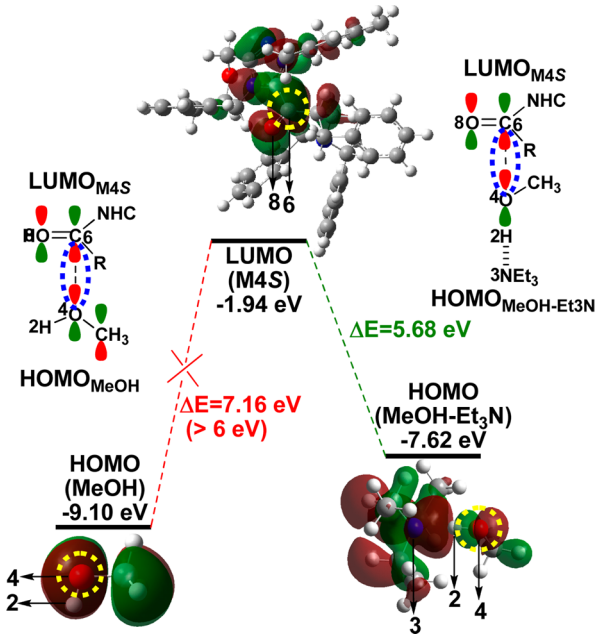

Figure 6. FMO interactions between $LUMO_{M4S}$ and $HOMO_{MeOH}$ or $HOMO_{MeOH\text{-}Et3N}$ calculated at the M06-2X/6-31G**//SMD_{DCM} level (unit: eV).

via the head-to-head mode to generate the new O4−C6 σ-bond (orbital) in this process. The FMO analysis shows that the HOMO energy of the MeOH-Et_3N complex is increased, when the MeOH is coordinated with Et_3N by a hydrogen bond, and the energy gap between the $LUMO_{M4S}$ and $HOMO_{MeOH\text{-}Et3N}$ is narrowed from 7.16 to 5.68 eV (Figure 6). Similarly, the bond order of O4−H2 in methanol is 0.59, while that in the MeOH-Et_3N complex is reduced to 0.57. These phenomena indicate that the Brønsted base plays two important roles in promoting the esterification reaction, i.e., one is to weaken the O−H bond and thus lower the energy barrier by HOMO-raising activation, and the other is a hydrogen acceptor to facilitate the proton abstraction.

3.4. Verification of the Computational Models. Based on the preceding discussions, we have disclosed the detailed mechanism of the novel cooperative organocatalytic reaction, revealed the factors that leading to high chemo- and enantioselectivity, and explored the roles of the catalysts. In order to further identify the reliability of our computational models to predict the stereoselectivities of the reaction, we have considered a series of α,β-unsaturated aldehydes with different substituent groups exhibiting diverse electronic and steric properties based on Chi's experiments.[14] The structural optimizations and energy calculations of the transition states involved in the enantioselectivity determining step (i.e., the C−C bond formation step) were performed in this part. In addition to **R1** (entry 1), the α,β-unsaturated aldehydes with electron-donating (entry 2) or electron-withdrawing (entry 3) groups, functional group (entry 4), heteroaryl groups (entries 5 and 6), β-ester (entry 7), or β-alkyl groups (entry 8) are examined in theory. As summarized in Table S4, the computed selectivities align well with the experimental observations, indicating that our computational model would be reliable to predict the stereoselectivity for this kind of reaction, and the

DOI: 10.1021/acs.joc.6b00656
J. Org. Chem. 2016, 81, 5370−5380

detailed discussions have been provided in the Supporting Information. Based on the NCI analysis, we think the stronger noncovalent interaction should be the fundamental factor in determining the enantioselectivity. In addition, we have provided and compared the NCI pictures of stereoselective transition states **TS4** with R^1 = CO_2Et and R^1 = Pyridine (see Figure S13 of Supporting Information); it should be noted that the noncovalent interactions are similar between the two transition states, which could reasonably explain the lower ee value in experiment. Additionally, it is obvious that the energy barriers would decrease when the nucleophilicities of the nucleophiles with different substituents in the same position increase (see Figure S11 of Supporting Information).

4. CONCLUSION

The detailed mechanisms and stereoselectivity of the NHC-BA/BB cooperatively catalyzed asymmetric aminomethylation reaction between *α,β*-unsaturated aldehyde and N,O-acetal have been investigated using DFT. On the whole, there are six elementary steps involved in tthe most energy favorable pathway, i.e., (1) nucleophilic addition of NHC to the *Si* face of **R1**, BA $Et_3N{\cdot}H^+$-assisted proton transfer processes for (2) the formation of the Breslow intermediate and (3) the subsequent *β*-protonation, (4) the Mannich reaction, (5) Brønsted base Et_3N-assisted esterification process to furnish the β^2-amino ester intermediate, and (6) the dissociation of the NHC catalyst from the final product. The fourth step is identified as the stereoselectivity-determining step, in which the *Si* face addition of *α*-carbon of the enolate intermediate by iminium cation **B** has been noted as the preferred mode, and finally leads to the *S* configuration product. Moreover, the analysis of energy span model shows that the *δE* of aminomethylation reaction is much smaller than that for self-redox reaction, so it is kinetically and thermodynamically favored, which is consistent with the experiment. The stronger *π*−*π* interaction in the favorable transition state (**TS5*S***) is the key for determining the enantioselectivity. In addition, the further calculations on the stereoselectivities of substrates with different substituent show that our computational model and results are reliable. All the calculations are in good agreement with experimental results.

Furthermore, we have explored the real roles of the catalysts by performing GRI analysis, and found that all the catalysts play very important roles during the fundamental reaction processes. The NHC catalyst plays a dual role: one is to activate the carbonyl C−H bond and the other is to serve as an LB catalyst to enhance the nucleophilicity of the reactant. For the in situ generated $Et_3N{\cdot}H^+$, two roles should be emphasized. One is the hydrogen bond donor to weaken the C−O bond, and the other is the protic mediator to lower the energy barrier of the proton transfer processes. Notably, the added base Et_3N (working as the hydrogen acceptor for HOMO-raising activation to weaken the O−H bond) has been found to be necessary for the esterification process, which is remarkably different from the previous NHC-BA cooperative catalysis reactions. As above, the computational results on the transition state models of the esterification process as well as the roles of catalysts should be useful for deeper understanding and rational design of this kind of cooperative NHC-BA/BB organocatalysis reaction.

■ ASSOCIATED CONTENT

Supporting Information

The Supporting Information is available free of charge on the ACS Publications website at DOI: 10.1021/acs.joc.6b00656.

Energy profiles of the whole reaction pathways, direct proton transfer, Et_3N-assisted proton transfer processes, and dimerization process; geometrical parameters involved in the proton transfer processes; details on the mediators-assisted proton transfer process; comparison of the Gibbs free energies of the stereoselective transition states calculated by M06-2X, *ω*B97X-D, B3LYP, and B3LYP-D3 methods using IEF-PCM and SMD salvation models; NBO charges of **R1** and ***Si*-M1**; scanning of distance C5−O4 between iminium cation **B** and MeO^-relationship between Nucleophilicity and HOMO energies of different substituents; Cartesian coordinates for all the optimized structures (PDF)

■ AUTHOR INFORMATION

Corresponding Author

*E-mail: donghuiwei@zzu.edu.cn

Notes

The authors declare no competing financial interest.

■ ACKNOWLEDGMENTS

The work described in this paper was supported by the National Natural Science Foundation of China (No. 21303167), China Postdoctoral Science Foundation (No. 2013M530340 and 2015T80776), Outstanding Young Talent Research Fund of Zhengzhou University (No.1521316001), and Excellent Doctoral Dissertation Engagement Fund of Zhengzhou University in 2014.

■ REFERENCES

(1) List, B. *Chem. Rev.* **2007**, *107*, 5413−5415.

(2) (a) Marcia de Figueiredo, R. M.; Christmann, M. *Eur. J. Org. Chem.* **2007**, *2007*, 2575−2600. (b) Marques-Lopez, E.; Herrera, R. P.; Christmann, M. *Nat. Prod. Rep.* **2010**, *27*, 1138−1167. (c) Grondal, C.; Jeanty, M.; Enders, D. *Nat. Chem.* **2010**, *2*, 167−178.

(3) Cheong, P. H. Y.; Legault, C. Y.; Um, J. M.; Celebi-Olcum, N.; Houk, K. N. *Chem. Rev.* **2011**, *111*, 5042−5137.

(4) Raup, D. E. A.; Cardinal-David, B.; Holte, D.; Scheidt, K. A. *Nat. Chem.* **2010**, *2*, 766−771.

(5) (a) Cohen, D. T.; Scheidt, K. A. *Chem. Sci.* **2012**, *3*, 53−57. (b) Wang, Z. Y.; Ding, Y. L.; Wang, G.; Cheng, Y. *Chem. Commun.* **2016**, *52*, 788−791. (c) Cardinal-David, B.; Raup, D. E. A.; Scheidt, K. A. *J. Am. Chem. Soc.* **2010**, *132*, 5345−5347.

(6) Mo, J. M.; Chen, X. K.; Chi, Y. R. *J. Am. Chem. Soc.* **2012**, *134*, 8810−8813.

(7) (a) Dugal-Tessier, J.; O'Bryan, E. A.; Schroeder, T. B. H.; Cohen, D. T.; Scheidt, K. A. *Angew. Chem., Int. Ed.* **2012**, *51*, 4963−4967. (b) Bera, S.; Daniliuc, C. G.; Studer, A. *Org. Lett.* **2015**, *17*, 4940−4943. (c) Bera, S.; Samanta, R. C.; Daniliuc, C. G.; Studer, A. *Angew. Chem., Int. Ed.* **2014**, *53*, 9622−9626. (d) Zhang, Y.; Lu, Y. Y.; Tang, W. F.; Lu, T.; Du, D. *Org. Biomol. Chem.* **2014**, *12*, 3009−3015. (e) Qi, J.; Xie, X. G.; Han, R. F.; Ma, D. H.; Yang, J.; She, X. G. *Chem. - Eur. J.* **2013**, *19*, 4146−4150.

(8) Xiao, Z. X.; Yu, C. X.; Li, T. J.; Wang, X. S.; Yao, C. S. *Org. Lett.* **2014**, *16*, 3632−3635.

(9) Fu, Z. Q.; Sun, H.; Chen, S. J.; Tiwari, B.; Li, G. H.; Chi, Y. R. *Chem. Commun.* **2013**, *49*, 261−263.

(10) Zhao, X. D.; DiRocco, D. A.; Rovis, T. *J. Am. Chem. Soc.* **2011**, *133*, 12466−12469.

DOI: 10.1021/acs.joc.6b00656
J. Org. Chem. 2016, 81, 5370−5380

(11) (a) Li, J. L.; Sahoo, B.; Daniliuc, C. G.; Glorius, F. *Angew. Chem., Int. Ed.* **2014**, *53*, 10515−10519. (b) Lin, Y. Q.; Yang, L. M.; Deng, Y.; Zhong, G. F. *Chem. Commun.* **2015**, *51*, 8330−8333. (c) Izquierdo, J.; Orue, A.; Scheidt, K. A. *J. Am. Chem. Soc.* **2013**, *135*, 10634−10637. (d) Tong, Y. F.; Mao, J. H.; Wu, S.; Zhao, Y.; Cheng, Y. *J. Org. Chem.* **2014**, *79*, 2075−2081. (e) Lee, A.; Scheidt, K. A. *Angew. Chem., Int. Ed.* **2014**, *53*, 7594−7598. (f) Youn, S. W.; Song, H. S.; Park, J. H. *Org. Lett.* **2014**, *16*, 1028−1031.
(12) Jin, Z. C.; Xu, J. F.; Yang, S.; Song, B. A.; Chi, Y. R. *Angew. Chem., Int. Ed.* **2013**, *52*, 12354−12358.
(13) Wang, M. H.; Cohen, D. T.; Schwamb, C. B.; Mishra, R. K.; Scheidt, K. A. *J. Am. Chem. Soc.* **2015**, *137*, 5891−5894.
(14) Xu, J. F.; Chen, X. K.; Wang, M.; Zheng, P. C.; Song, B. A.; Chi, Y. R. *Angew. Chem., Int. Ed.* **2015**, *54*, 5161−5165.
(15) Wang, Y.; Wu, B. H.; Zheng, L. J.; Wei, D. H.; Tang, M. S. *Org. Chem. Front.* **2016**, *3*, 190−203.
(16) (a) Wang, Y.; Zheng, L. J.; Wei, D. H.; Tang, M. S. *Org. Chem. Front.* **2015**, *2*, 874−884. (b) Li, Z. Y.; Wei, D. H.; Wang, Y.; Zhu, Y. Y.; Tang, M. S. *J. Org. Chem.* **2014**, *79*, 3069−3078.
(17) Wang, Y. Y.; Wei, D. H.; Wang, Y.; Zhang, W. J.; Tang, M. S. *ACS Catal.* **2016**, *6*, 279−289.
(18) Liang, Y.; Liu, S.; Yu, Z. X. *Synlett* **2009**, *2009*, 905−909.
(19) (a) Zhang, M. M.; Wei, D. H.; Wang, Y.; Li, S. J.; Liu, J. F.; Zhu, Y. Y.; Tang, M. S. *Org. Biomol. Chem.* **2014**, *12*, 6374−6383. (b) Wei, D. H.; Zhu, Y. Y.; Zhang, C.; Sun, D. Z.; Zhang, W. J.; Tang, M. S. *J. Mol. Catal. A: Chem.* **2011**, *334*, 108−115.
(20) (a) Hao, L.; Du, Y.; Lv, H.; Chen, X. K.; Jiang, H. S.; Shao, Y. L.; Chi, Y. R. *Org. Lett.* **2012**, *14*, 2154−2157. (b) Fu, Z. Q.; Xu, J. F.; Zhu, T. S.; Leong, W. W. Y.; Chi, Y. R. *Nat. Chem.* **2013**, *5*, 835−839. (c) Zhu, T. S.; Mou, C. L.; Li, B. S.; Smetankova, M.; Song, B. A.; Chi, Y. R. *J. Am. Chem. Soc.* **2015**, *137*, 5658−5661. (d) Liu, R.; Yu, C. X.; Xiao, Z. X.; Li, T. J.; Wang, X. S.; Xie, Y. W.; Yao, C. S. *Org. Biomol. Chem.* **2014**, *12*, 1885−1891. (e) Wang, M.; Huang, Z. J.; Xu, J. F.; Chi, Y. R. *J. Am. Chem. Soc.* **2014**, *136*, 1214−1217. (f) Jin, Z. C.; Chen, S. J.; Wang, Y. H.; Zheng, P. C.; Yang, S.; Chi, Y. R. *Angew. Chem., Int. Ed.* **2014**, *53*, 13506−13509. (g) Reddi, Y.; Sunoj, R. B. *ACS Catal.* **2015**, *5*, 5794−5802.
(21) (a) Sohn, S. S.; Rosen, E. L.; Bode, J. W. *J. Am. Chem. Soc.* **2004**, *126*, 14370−14371. (b) Burstein, C.; Glorius, F. *Angew. Chem., Int. Ed.* **2004**, *43*, 6205−6208. (c) Han, R. F.; Qi, J.; Gu, J. X.; Ma, D. H.; Xie, X. G.; She, X. G. *ACS Catal.* **2013**, *3*, 2705−2709.
(22) (a) Zhang, W. J.; Zhu, Y. Y.; Wei, D. H.; Li, Y. X.; Tang, M. S. *J. Org. Chem.* **2012**, *77*, 10729−10737. (b) Zhang, W. J.; Wei, D. H.; Tang, M. S. *J. Org. Chem.* **2013**, *78*, 11849−11859. (c) Qiao, Y.; Wei, D. H.; Chang, J. B. *J. Org. Chem.* **2015**, *80*, 8619−8630.
(23) (a) Reddi, Y.; Sunoj, R. B. *ACS Catal.* **2015**, *5*, 1596−1603. (b) Reddi, Y.; Sunoj, R. B. *Org. Lett.* **2012**, *14*, 2810−2813. (c) Kuniyil, R.; Sunoj, R. B. *Org. Lett.* **2013**, *15*, 5040−5043.
(24) Frisch, M. J.; Trucks, G. W.; Schlegel, H. B.; Scuseria, G. E.; Robb, M. A.; Cheeseman, J. R.; Scalmani, G.; Barone, V.; Mennucci, B.; Petersson, G. A.; Nakatsuji, H.; Caricato, M.; Li, X.; Hratchian, H. P.; Izmaylov, A. F.; Bloino, J.; Zheng, G.; Sonnenberg, J. L.; Hada, M.; Ehara, M.; Toyota, K.; Fukuda, R.; Hasegawa, J.; Ishida, M.; Nakajima, T.; Honda, Y.; Kitao, O.; Nakai, H.; Vreven, T.; Montgomery, J. A., Jr.; Peralta, J. E.; Ogliaro, F.; Bearpark, M.; Heyd, J. J.; Brothers, E.; Kudin, K. N.; Staroverov, V. N.; Kobayashi, R.; Normand, J.; Raghavachari, K.; Rendell, A.; Burant, J. C.; Iyengar, S. S.; Tomasi, J.; Cossi, M.; Rega, N.; Millam, J. M.; Klene, M.; Knox, J. E.; Cross, J. B.; Bakken, V.; Adamo, C.; Jaramillo, J.; Gomperts, R.; Stratmann, R. E.; Yazyev, O.; Austin, A. J.; Cammi, R.; Pomelli, C.; Ochterski, J. W.; Martin, R. L.; Morokuma, K.; Zakrzewski, V. G.; Voth, G. A.; Salvador, P.; Dannenberg, J. J.; Dapprich, S.; Daniels, A. D.; Farkas, O.; Foresman, J. B.; Ortiz, J. V.; Cioslowski, J.; Fox, D. J. *Gaussian 09*, Revision C.01; Gaussian, Inc.; Wallingford, CT, 2010.
(25) (a) Wang, Y.; Wei, D. H.; Li, Z. Y.; Zhu, Y. Y.; Tang, M. S. *J. Phys. Chem. A* **2014**, *118*, 4288−4300. (b) Wang, Y.; Guo, X. K.; Tang, M. S.; Wei, D. H. *J. Phys. Chem. A* **2015**, *119*, 8422−8431. (c) Wu, J. C.; Xu, W. B.; Yu, Z. X.; Wang, J. *J. Am. Chem. Soc.* **2015**, *137*, 9489−9496. (d) Xu, L. P.; Chung, L. W.; Wu, Y. D. *ACS Catal.* **2016**, *6*, 483−493. (e) Guo, X. K.; Zhang, L. B.; Wei, D. H.; Niu, J. L. *Chem. Sci.* **2015**, *6*, 7059−7071. (f) Xing, Y. M.; Zhang, L.; Fang, D. C. *Organometallics* **2015**, *34*, 770−777. (g) Zhang, L.; Wang, Y.; Yao, Z. J.; Wang, S. Z.; Yu, Z. X. *J. Am. Chem. Soc.* **2015**, *137*, 13290−13300.
(26) (a) Wei, D. H.; Lei, B. L.; Tang, M. S.; Zhan, C. G. *J. Am. Chem. Soc.* **2012**, *134*, 10436−10450. (b) Qiao, Y.; Han, K. L.; Zhan, C. G. *Biochemistry* **2013**, *52*, 6467−6479.
(27) (a) Zhao, Y.; Truhlar, D. G. *Theor. Chem. Acc.* **2008**, *120*, 215−241. (b) Zhao, Y.; Truhlar, D. G. *Acc. Chem. Res.* **2008**, *41*, 157−167.
(28) (a) Marenich, A. V.; Cramer, C. J.; Truhlar, D. G. *J. Phys. Chem. B* **2009**, *113*, 6378−6396. (b) Marenich, A. V.; Cramer, C. J.; Truhlar, D. G. *J. Phys. Chem. B* **2009**, *113*, 4538−4543.
(29) (a) Gonzalez, C.; Schlegel, H. B. *J. Chem. Phys.* **1989**, *90*, 2154−2161. (b) Gonzalez, C.; Schlegel, H. B. *J. Phys. Chem.* **1990**, *94*, 5523−5527.
(30) (a) Reed, A. E.; Weinhold, F. J. *J. Chem. Phys.* **1983**, *78*, 4066−4073. (b) Foster, J. P.; Weinhold, F. J. *J. Am. Chem. Soc.* **1980**, *102*, 7211−7218. (c) Glendening, E. D.; Reed, A. E.; Carpenter, J. E.; Weinhold, F. J. *NBO* v 3.1.
(31) Legault, C. Y. *CYLview*, v 1.0b; Université de Sherbrooke, 2009; http://www.cylview.org.
(32) Chai, J. D.; Head-Gordon, M. *Phys. Chem. Chem. Phys.* **2008**, *10*, 6615−6620.
(33) (a) Becke, A. D. *J. Chem. Phys.* **1993**, *98*, 5648−5652. (b) Lee, C. T.; Yang, W. T.; Parr, R. G. *Phys. Rev. B: Condens. Matter Mater. Phys.* **1988**, *37*, 785−789. (c) Miehlich, B.; Savin, A.; Stoll, H.; Preuss, H. *Chem. Phys. Lett.* **1989**, *157*, 200−206.
(34) Grimme, S.; Ehrlich, S.; Goerigk, L. *J. Comput. Chem.* **2011**, *32*, 1456−1465.
(35) (a) Wang, Y.; Wei, D. H.; Zhang, W. J.; Wang, Y. Y.; Zhu, Y. Y.; Jia, Y.; Tang, M. S. *Org. Biomol. Chem.* **2014**, *12*, 7503−7514. (b) Liang, Y.; Zhou, H. L.; Yu, Z. X. *J. Am. Chem. Soc.* **2009**, *131*, 17783−17785. (c) Xia, Y. Z.; Liang, Y.; Chen, Y. Y.; Wang, M.; Jiao, L.; Huang, F.; Liu, S.; Li, Y. H.; Yu, Z. X. *J. Am. Chem. Soc.* **2007**, *129*, 3470−3471. (d) Shi, F. Q.; Li, X.; Xia, Y.; Zhang, L.; Yu, Z. X. *J. Am. Chem. Soc.* **2007**, *129*, 15503−15512.
(36) (a) Kozuch, S.; Shaik, S. *Acc. Chem. Res.* **2011**, *44*, 101−110. (b) Wang, Y.; Guo, X. K.; Wu, B. H.; Wei, D. H.; Tang, M. S. *RSC Adv.* **2015**, *5*, 100147−100158.
(37) Lu, T.; Chen, F. W. *J. Comput. Chem.* **2012**, *33*, 580−592.
(38) (a) Parr, R. G.; Pearson, R. G. *J. Am. Chem. Soc.* **1983**, *105*, 7512−7516. (b) Domingo, L. R.; Picher, M. T.; Saez, J. A. *J. Org. Chem.* **2009**, *74*, 2726−2735.
(39) (a) Domingo, L. R.; Perez, P.; Saez, J. A. *RSC Adv.* **2013**, *3*, 1486−1494. (b) Domingo, L. R.; Chamorro, E.; Perez, P. *Eur. J. Org. Chem.* **2009**, *2009*, 3036−3044. (c) Domingo, L. R.; Chamorro, E.; Perez, P. *J. Phys. Chem. A* **2008**, *112*, 4046−4053.
(40) Zhuo, L. G.; Liao, W.; Yu, Z. X. *Asian J. Org. Chem.* **2012**, *1*, 336−345.

DOI: 10.1021/acs.joc.6b00656
J. Org. Chem. 2016, 81, 5370−5380